HHS Public Access

Author manuscript

Nat Methods. Author manuscript; available in PMC 2019 February 28.

Published in final edited form as:

Nat Methods. 2018 September ; 15(9): 669–676. doi:10.1038/s41592-018-0085-0.

Precision and accuracy of single-molecule FRET measurements – a multi-laboratory benchmark study

A full list of authors and affiliations appears at the end of the article.

Abstract

Single-molecule Förster resonance energy transfer (smFRET) is increasingly being used to determine distances, structures, and dynamics of biomolecules *in vitro* and *in vivo*. However, generalized protocols and FRET standards ensuring the reproducibility and accuracy of measuring FRET efficiencies are currently lacking.

Here we report the results of a worldwide, comparative, blind study, in which 20 labs determined the FRET efficiencies, *E,* of several dye-labeled DNA duplexes. Using a unified and straightforward method, we show that FRET efficiencies can be obtained with a standard deviation between $\Delta E = \pm 0.02$ and ± 0.05. We suggest an experimental and computational procedure for converting FRET efficiencies into accurate distances. We discuss potential uncertainties in the experiment and the modeling. Our extensive quantitative assessment of intensity-based smFRET measurements and correction procedures are an essential step towards validation of distance networks with the ultimate aim to achieve reliable structural models of biomolecular systems obtained by smFRET-based hybrid methods.

Introduction

Förster Resonance Energy Transfer (FRET) [1], also termed Fluorescence Resonance Energy Transfer, has become a well-established method for studying biomolecular conformations and dynamics at both the ensemble [2–4] and the single-molecule (sm) level [5–10]. In such experiments, the energy transfer between a donor and an acceptor fluorophore pair is

*corresponding authors: jens.michaelis@uni-ulm.de; cseidel@hhu.de; t.craggs@sheffield.ac.uk; thorsten.hugel@pc.uni-freiburg.de.
°these authors contributed equally

Author Contributions

B.H., T.H., J.M., C.S. designed the research; B.H., S.S., O.D., O.O., R.K., S.R.A., B.A., M.A., A.B., H.C., T.E., C.F., C.G., G.G., P.H., C.A.H., A.H., J.H., L.L.H., V.H., J.H., B.H., E.K., J.K., G.K., B.L., J.J.M., N.N., D.N., T.N., R.Q., N.C.R., C.R., T.S., H.S., L.S., J.T., S.T., N.V., A.M.V., B.W., I.S.Y. and T.D.C. performed measurements; B.H., S.S. and T.H. compared the measurements; all authors contributed to the analysis of the data and commented on the manuscript; B.H., S.S., T.D.C., J.M., C.S. and T.H. wrote the manuscript in consultation with O.D. and O.O. O.D. performed the calculations of the model distances.

Competing financial interests

The authors declare no competing financial interests.

Data availability

All data is available from the corresponding authors upon request. The raw data for Fig. 2 is available at Zenodo: http://doi.org/10.5281/zenodo.1249497.

Code availability

All custom code used herein is available from the authors upon request.

quantified with respect to their proximity [1]. The fluorophores are usually attached via flexible linkers to defined positions of the system under investigation. The transfer efficiency depends on the inter-dye distance, which is well-described by Förster's theory for distances > 30 Å [11,12]. Accordingly, FRET has been termed a 'spectroscopic ruler' on the molecular scale[2]. Such a ruler is an important tool to determine distances *in vitro,* and even in cells [13], with potentially Ångström accuracy and precision. In its single-molecule implementation, FRET largely overcomes ensemble- and time-averaging and can uncover individual species within heterogeneous and dynamic biomolecular complexes, as well as transient intermediates[5].

The two most popular smFRET approaches to determine distances are confocal microscopy on freely diffusing molecules, and total internal reflection fluorescence (TIRF) microscopy on surface-attached molecules. Various fluorescence intensity- and lifetime-based procedures have been proposed with the aim of determining FRET efficiencies [10,14–20]. Here, we focus on intensity-based measurements, in which the FRET efficiency, E, is determined from donor and acceptor photon counts, and then subsequently used to calculate the inter-fluorophore distance according to Förster's theory. Specifically, we discuss solution-based measurements using a confocal microscope, and surface-based measurements using a TIRF microscope.

The vast majority of intensity-based smFRET studies to date rely on characterizing relative changes in FRET efficiency. This ratiometric approach is often sufficient to distinguish different conformations of a biomolecule (e.g. an open conformation with low FRET efficiency vs. a closed conformation with high FRET efficiency), and to determine their interconversion kinetics. Yet, determining distances provides additional information that can be used, for example, to compare with known structures, or assign conformations to different structural states. In combination with prior structural knowledge and computer simulations, FRET-derived distances are increasingly being used to generate novel biomolecular structural models using hybrid structural tools [7–9,21–26].

However, comparing and validating distance measurements from different labs is difficult, especially given the lack of detailed methodological descriptions in many publications. In addition, different methods for data acquisition and analysis, often using home-built microscopes with in-house software, can have very different uncertainties and specific pitfalls. To overcome these issues, we have developed general methodological recommendations and well-characterized FRET-standard samples to enable the validation of results and the estimation of distance accuracy and precision. This approach should allow the scientific community to confirm the consistency of smFRET-derived distances and structural models. To facilitate data validation across the field, we recommend the reporting of specific FRET-related parameters with a unified nomenclature.

The presented step-by-step procedure for obtaining FRET efficiencies and relevant correction parameters is tested in a worldwide, comparative, blind study by 20 participating labs. For standardized FRET samples, we show that FRET efficiencies can be determined with a standard deviation $\Delta E < \pm 0.05$.

In order to convert the measured smFRET efficiency to a distance, the Förster equation is used (*Online Methods* eq.3), which critically depends on the dye-pair-specific Förster radius, R_0. We discuss the measurements required to determine R_0 and the associated uncertainties. Another uncertainty arises from the fact that many positions are being sampled by the dye relative to the biomolecule to which it is attached. Therefore, specific models are used to describe the dynamic movement of the dye molecule, during the recording of each FRET-efficiency measurement [22,23]. The investigation of the uncertainties in FRET-efficiency determination and the conversion into distances enables us to specify uncertainties for individual FRET-derived distances.

We anticipate that the investigated samples and the presented procedure will help unify the research field, serving as a standard for future publications and benchmarking the use of smFRET as an accurate spectroscopic ruler.

Results

Benchmark samples and approaches

We have chosen double-stranded DNA as a FRET standard for the following reasons: any DNA sequence can be synthesized; FRET dyes can be specifically tethered at desired positions; the structure of B-form DNA is well characterized; and the samples are stable at room temperature for a time window that is large enough for shipping to labs around the world. The donor and acceptor dyes are attached via C2- or C6-amino-linkers to thymidines of opposite strands (see Supplementary Figure 1). These thymidines were separated either by 23 or 15 base pairs (Figure 1 and *Online Methods section2*) and 11 base pairs in a follow-up study (see Supplementary Table 1 and Supplementary Note 1). The attachment positions were known only to the reference lab that designed the samples. Based on the resulting lo-, mid- and hi- FRET-efficiency samples, respectively, we were able to determine all correction parameters and to perform a self-consistency test (see below).

In this study we used Alexa and Atto dyes (Supplementary Figure 1) due to their high quantum yields and well-studied characteristics (Supplementary Note 2). Eight hybridized double-stranded FRET samples were shipped to all participating labs. In the main text, we focus on four FRET samples that were measured by most labs in our study (see *Online Methods section2* for details):

1-lo: Atto550/Atto647N, 23 bp-separation.

1-mid: Atto550/Atto647N, 15 bp-separation.

2-lo: Atto550/Alexa647, 23 bp-separation.

2-mid: Atto550/Alexa647, 15 bp-separation.

In this nomenclature, the number refers to the dye pair and the letters indicate either the low-efficiency (lo) or medium-efficiency (mid) configurations. The results with other FRET pairs (Alexa488/Alexa594 and Alexa488/Atto647N) at these positions are reported in Supplementary Figure 2 and Supplementary Note 2. During revision, we conducted a further blind study involving 13 labs and a third set of samples:

1-hi: Atto550/Atto647N, 11 bp-separation.

2-hi: Atto550/Alexa647, 11 bp-separation.

The results per lab for all samples are reported in Supplementary Figure 2.

In order to avoid dye stacking[28,29], we designed the DNA molecules such that the dyes are attached to internal positions sufficiently far from the duplex ends. As a first test for the suitability of the labels, we checked the fluorescence lifetimes and time-resolved anisotropies (Supplementary Table 2) of all donor-only and acceptor-only samples. The results indicate that there is no significant quenching or stacking and that all dyes are sufficiently mobile at these positions (see Supplementary Note 2).

Most measurements were performed on custom-built setups featuring at least two separate spectral detection channels for donor and acceptor emission (Supplementary Figures 3 and 4). For results obtained using different fluorophores (samples 3 and 4) and different FRET methods (ensemble lifetime [30], single-molecule lifetime [16], and a phasor approach [31]) see Supplementary Figure 2 and Supplementary Note 1 and 2).

The first challenge is a robust correction procedure to obtain absolute fluorescence intensities. The ideal solution is a ratiometric approach which for intensity-based confocal FRET measurements was pioneered by Weiss and coworkers using alternating two-color laser excitation (ALEX) with microsecond pulses[17,32]. In this approach the fluorescence signal after donor excitation is divided by the total fluorescence signal after donor and acceptor excitation (referred to as apparent stoichiometry, see eqn.16), to correct for dye and instrumental properties [17]. The ALEX approach was also adapted for TIRF measurements [20]. To increase time resolution and to enable time-resolved spectroscopy, Lamb and coworkers introduced pulsed interleaved excitation (PIE) with picosecond pulses [33].

Procedure to determine the experimental FRET efficiency $\langle E \rangle$

In both confocal and TIRF microscopy, the expectation value of the FRET efficiency $\langle E \rangle$ is computed from the corrected FRET efficiency histogram. First, we describe a concise and robust procedure to obtain $\langle E \rangle$. Then we perform distance and uncertainty calculations, assuming a suitable model for the inter-dye distance distribution and dynamics [6,11,34]. Further, we derive self-consistency arguments and comparisons to structural models and thereby confirm the accuracy of this method.

Our general procedure is largely based on the Lee et al. approach [17], with modifications to establish a robust workflow and standardize the nomenclature. Intensity-based determination of FRET efficiencies requires the consideration of the following correction factors (see *Online Methods, section1*): Background signal correction (BG) from donor and acceptor channels; factor for spectral crosstalk (α), arising from donor fluorescence leakage in the acceptor channel; factor for direct excitation (δ) of the acceptor with the donor laser; detection correction factor (γ). The optimal way to determine these factors is by alternating the excitation between two colors, which allows for the determination of the FRET efficiency (E) and the relative stoichiometry (S) of donor and acceptor dyes, for each single-

molecule event. This introduces the additional excitation correction factor (β) to normalize the excitation rates (see *Online Methods section3.6*).

The following step-by-step guide is subdivided for confocal and TIRF experiments; notably, the order of the steps is crucial (see *Online Methods section3* for details).

Diffusing molecules: Confocal Microscopy—Photon arrival times from individual molecules freely diffusing through the laser focus of a confocal microscope are registered. Applying signal threshold criteria, bursts are collected and analyzed. From the data, first a 2D histogram of the uncorrected FRET efficiency ($^{i}E_{app}$) versus uncorrected stoichiometry ($^{i}S_{app}$) is calculated (Figure 2a). Then, the average number of background photons is subtracted for each channel separately (Figure 2b). Next, to obtain the FRET sensitized acceptor signal ($F_{A|D}$), donor leakage ($\alpha^{ii}I_{Dem|Dex}$) and direct excitation ($\delta^{ii}I_{Aem|Aex}$) must be subtracted from the acceptor signal after donor excitation. As samples never contain 100% photoactive donor and acceptor dyes, the donor- and acceptor-only populations are selected from the measurement and used to determine the leakage and direct excitation (Figure 2c)). After this correction step, the donor-only population should have an average FRET efficiency of 0 and the acceptor-only population should have an average stoichiometry of 0.

The last step deals with the detection correction factor γ and the excitation correction factor β. If at least two species (two different samples or two populations within a sample) with different inter-dye distances are present, they can be used to obtain the "*global γ-correction*". If one species with significant distance fluctuations, e.g. through intrinsic conformational changes, is present a "*single-species γ-correction*" may be possible. Both correction schemes assume that the fluorescence quantum yields and extinction coefficients of the dyes are independent of the attachment point (see *Online Methods section3.6*). The correction factors obtained by the reference lab are compiled in Supplementary Table 3. The final corrected FRET efficiency histograms are shown in Figure 2d. The expected efficiencies $\langle E \rangle$ are obtained as the mean of a Gaussian fit to the respective efficiency distributions.

Surface-attached molecules: TIRF Microscopy—The correction procedure for TIRF-based smFRET experiments is similar to the procedure for confocal-based experiments. In the procedure used for ALEX data [20], a 2D histogram of the uncorrected FRET efficiency ($^{i}E_{app}$) versus uncorrected stoichiometry ($^{i}S_{app}$) is first generated (Figure 2e). The background subtraction is critical in TIRF microscopy as it can contribute significantly to the measured signal. Different approaches can be used to accurately determine the background signal (see *Online Methods section3.3*), such as measuring the background in the vicinity of the selected particle or measuring the intensity after photobleaching (Figure 2f). After background correction, the leakage and direct excitation can be calculated from the ALEX data as for confocal microscopy (Figure 2g).

Again, determination of the correction factors β and γ are critical[15]. As in confocal microscopy, one can use the stoichiometry information available from ALEX when multiple populations are present to determine an average detection correction factor (*global γ-*

correction). In TIRF microscopy, the detection correction factor can also be determined on a molecule-by-molecule basis, provided the acceptor photobleaches before the donor (*individual γ-correction*). In this case, the increase in the fluorescence of the donor can be directly compared to the intensity of the acceptor before photobleaching. A 2D histogram of the corrected FRET efficiency versus the corrected stoichiometry is shown in Figure 2h.

In the absence of alternating laser excitation, the following problems were occasionally encountered during this study: (i) the low-FRET efficiency values were shifted systematically to higher efficiencies, because FRET efficiency values at the lower edge are overlooked due to noise; (ii) the direct excitation was difficult to detect and correct, due to its small signal to noise ratio; (iii) the acceptor bleaching was difficult to detect for low FRET efficiencies. Therefore, implementation of ALEX is strongly recommended for obtaining accurate FRET data.

Nine of the twenty participating labs determined FRET efficiencies by confocal methods for sample 1 and 2 (Figure 3a). Seven of the twenty participating labs determined FRET efficiencies by TIRF-based methods and these are summarized in Figure 3b. The combined data from all labs measuring samples 1 and 2 agree very well, with a standard deviation for the complete data set of $\Delta E<\pm 0.05$. This is a remarkable result, considering that different setup types were used (confocal- and TIRF-based setups) and different correction procedures were applied (e.g. individual, global or single species γ-correction).

Distance determination

The ultimate goal is to derive distances from the FRET efficiencies. The efficiency-distance conversion requires both the knowledge of the Förster radius, R_0, for the specific FRET pair used, and a specific dye model, describing the behavior of the dye attached to the macromolecule[22,23]. In the following, we describe (i) how R_0 can be determined and (ii) how to use a specific dye model to calculate the $R(\langle E \rangle)$ referred to as $R_{\langle E \rangle}$ and the R_{MP}. $R_{\langle E \rangle}$ is the apparent donor-acceptor distance, which is directly related to the experimental FRET efficiency $\langle E \rangle$, that is averaged over all sampled donor acceptor distances R_{DA} (eq.5), but it is not a physical distance. R_{MP} is the real distance between the center points (mean positions) of the accessible volumes and deviates from $R_{\langle E \rangle}$ because of the different averaging in distance and efficiency space. R_{MP} cannot be directly measured, but is important, for example, for mapping the physical distances required for structural modeling [34].

R_0 is a function of (eq.7): the index of refraction of the medium between the two fluorophores (n_{im}), the spectral overlap integral (J), the fluorescence quantum yield of the donor ($\Phi_{F,D}$), and the relative dipole orientation factor (κ^2) (see *Online Methods section4*, for an estimate of their uncertainties). Our model assumes that the FRET rate (k_{FRET}) is much slower than the rotational relaxation rate (k_{rot}) of the dye and that the translational diffusion rate (k_{diff}) allows the dye to sample the entire accessible volume within the experimental integration time ($1/k_{int}$), i.e. $k_{rot} \gg k_{FRET} \gg k_{diff} \gg k_{int}$. The validity of these assumptions is justified by experimental observables discussed in the *Online Methods section4.4*.

The determined Förster radii for sample 1 and sample 2 are given in Supplementary Table 4. Note that literature values differ mainly because donor fluorescence quantum yields are not specified and the refractive index of water is often assumed, while we used $n_{im} = 1.40$ here (see *Online Methods section4.1*). Our careful error analysis led to an error estimate of 7% for the determined R_0, which is relatively large (mainly due to the uncertainty in κ^2).

We used the measured smFRET efficiencies and the calculated Förster radii to compute the apparent distance $R_{\langle E \rangle}$ from each lab's data (eq.5). Figure 4a+b shows the calculated values for these apparent distances for sample 1 and 2 for each data point in Figure 3. The average values for all labs are given in Supplementary Table 4 together with model values based on the knowledge of the dye attachment positions, the static DNA structure and the mobile dye model (Supplementary Note 3). Considering the error ranges, the experimental and model values agree very well with each other (the deviations range between 0 and 8 %).

Whilst this study focused on measurements on DNA, the described FRET analysis and error estimation are fully generalizable to other systems (e.g. proteins) assuming mobile dyes. What becomes more difficult for proteins is specific dye-labeling, and the determination of an appropriate dye-model, if the dyes are not sufficiently mobile (see S*upplementary Note 4*).

$R_{\langle E \rangle}$ only corresponds to the real distance R_{MP} in the hypothetical case in which both dyes are unpolarized point sources, with zero accessible volume (AV). In all other cases, R_{MP} is the only physical distance. It can be calculated in two ways: (i) If the dye model and the local environment of the dye is known (see Figure 1), simulation tools such as the FPS [8] can be used to compute the R_{MP} from $R_{\langle E \rangle}$ for a given pair of AVs. (ii) If the structure of the investigated molecule is unknown *a priori*, a sphere is a useful assumption for the AV. In both cases, a lookup table serves to convert $R_{\langle E \rangle}$ to R_{MP} for defined AVs and R_0's (Supplementary Note 5). The results, given as distances determined using the former approach, are shown in Figures 4c+d and Supplementary Table 4. The respective model values are based on the center points of the AVs depicted in Figure 1 and given in Supplementary Table 4 (see Supplementary Note 3 for details).

Distance uncertainties

We estimated all uncertainty sources arising from both the measurement of the corrected FRET efficiencies and the determination of the Förster radius, and propagated them into distance uncertainties. First, we discuss the error in determining the distance between two freely rotating but spatially fixed dipoles, R_{DA}, with the Förster equation (eq. 26). Figure 5a shows how uncertainties in each of the correction factors (α, γ, δ) and the background signals (BG_D, BG_A) translate into the uncertainty of R_{DA} (see Supplementary Note 6 for all equations). The uncertainty of R_{MP} is similar, but depends on the dye model and the AVs. The solid gray line shows the sum of these efficiency-dependent uncertainties, which are mainly setup-specific quantities. For the extremes of the distances the largest contribution to the uncertainty in R_{DA} arises from background photons in the donor and acceptor channels. In the presented example with $R_0 = 62.6$ Å the total uncertainty ΔR_{DA} based on the *setup-specific uncertainties* is less than 4 Å for 35 Å < R_{DA} < 90 Å. Notably, in confocal measurements, larger intensity thresholds can decrease this uncertainty further. The

uncertainty in R_{DA} arising from errors in R_0 (blue line in Figure 5b) is added to the efficiency-related uncertainty in R_{DA} (bold gray line) to estimate the total experimental uncertainty in R_{DA} ($\Delta R_{DA,total}$, black line). The uncertainties for determining R_0 are dominated by the dipole orientation factor κ^2 and the refractive index n_{im} (*Online Methods section 3)*. Including the uncertainty in R_0, the error $\Delta R_{DA,total}$ for a single smFRET-based distance between two freely rotating point dipoles is less than 6 Å for 35 Å < R_{DA} < 80 Å. The uncertainty is considerably reduced when multiple distances are calculated and self-consistency in distance networks is exploited [9]. Besides background contributions, an R_{DA} shorter than 30 Å may be prone to larger errors due to: (i) potential dye-dye interactions (ii) the dynamic averaging of the dipole orientations being reduced due to an increased FRET rate.

Comparing distinct dye pairs

In order to validate the model assumption of a freely rotating and diffusing dye we developed a self-consistency argument based on the relationship between different dye pairs that bypasses several experimental uncertainties. We define the ratio, R_{rel}, for two dye pairs as the ratio of their respective $R_{\langle E \rangle}$ values (see *Online Methods* eq.30). This ratio is quasi-independent of R_0, because all dye parameters that are contained in R_0 are approximately eliminated using our DNA design. Therefore these ratios should be similar for all investigated dye-pairs, which is indeed the case (Supplementary Table 4). When comparing e.g. the lo- to mid-distance for the three dye pairs with E > 0.1, we obtain a mean R_{rel} of 1.34 and a maximum deviation of 2.7%. This is a relative error of 2.3% and thus below the estimated error of our measured distances of 2.8% (Figure 5a). This further demonstrates the validity of the assumptions for the dye model and averaging regime used here. For further discussion see the *Online Methods section4.7*. While the analysis in this paper used a static model for the DNA structure, DNA is known not to be completely rigid [35]. We tested our DNA model by performing MD simulations of the DNA molecule (without attached dye molecules, see Supplementary Note 7) and found that the averaged expected FRET efficiency using the computed dynamically-varying slightly bent DNA structure leads to comparable but slightly longer distances than for the static model. The deviations between the models and data are reduced (Supplementary Table 4) for those cases where larger deviations were observed using static models.

Discussion

The reported intensity-based FRET efficiencies are consistent throughout the labs, despite using different setup types. This remarkable consistency (ΔE < ±0.05) was achieved by applying a general step-by-step procedure to perform the experiment and analyze the data.

We also showed that the factors required for correcting the FRET efficiency can be determined with high precision, independent of the different setup types and acquisition software used. Together the measurement errors in the correction factors cause an uncertainty in R_{DA} of less than 5 %, which agrees well with the variations observed between the reported results from the different labs. Ultimately, we are interested in the absolute distances derived from these FRET measurements. Figure 5 shows that any distance between

0.6 R_0 and 1.6 R_0 can be determined with an uncertainty of less than ±6 Å in the distance range from 35 to 80 Å for the dye-pairs used in sample 1. This estimation is valid if the dyes are sufficiently mobile which has been supported by time-resolved anisotropy measurements and further confirmed by a self-consistency argument. For sample 2 the standard deviation is slightly larger than for sample 1 (see Figure 5a), which could be explained by dye specific photophysical properties. The values for samples 3 and 4 (Supplementary Table 4) show similar precision, considering the smaller number of measurements (N).

For the samples 1-hi and 2-hi, which were measured later after each lab verified their setup and procedure, the precision was further increased by almost a factor of two (see Supplementary Table 4), possibly due to the thorough characterization during this study.

In addition to the achievable precision, we also tested the accuracy of the experimentally derived distances by comparing them with distances of the static model. For every *single* FRET pair we found an excellent agreement between 0.1% and 4.1% (0.4–2.4 Å) for sample 1 and an agreement mostly within experimental error between 3.1% to 9.0% (2.7–5.5 Å) for sample 2. The deviations can be even smaller for dynamic DNA models. For sample 2, which had the cyanine-based dye Alexa647 instead of the carbopyronine-based dye Atto647N as an acceptor, the lower accuracy could be explained by an imperfect sampling of the full AV or dye specific photophysical properties (for details see Supplementary Table 2). Previously it has been shown that cyanine dyes are sensitive to their local environment[36] and therefore require especially careful characterization for each newly labeled biomolecule.

For future work, it will be powerful to complement intensity-based smFRET studies with sm-lifetime studies because the picosecond time resolution can provide additional information on calibration and fast dynamic biomolecular exchange. In addition, it will be important to establish appropriate dye models for more complex (protein) systems, in which the local chemistry may affect dye mobility (Supplementary Note 4). However, for the case of mobiles dyes (which can be checked by anisotropy and lifetime experiments - see Supplementary Note 2) the dye model here is fully generalizable to any biomolecular system [8,9].

The results from different labs and the successful self-consistency test clearly show the great potential of absolute smFRET-based distances for investigating biomolecular conformations and dynamics, as well as for integrative structural modeling. The ability to accurately determine distances on the molecular scale with smFRET experiments and to estimate the uncertainty of the measurements, provides the groundwork for smFRET-based structural and hybrid approaches. Together with the automated selection of the most informative pairwise labeling positions [23], and fast analysis procedures [8–10], we anticipate smFRET-based structural methods will become an important tool for *de novo* structural determination and structure validation, especially for large and flexible structures where other structural biology methods are difficult to apply.

Online Methods

1 Nomenclature and Definitions

See Supplementary Table 5 for a probably more convenient version of this first section of the Online Methods.

The FRET efficiency E is:

$$E = \frac{F_{A \mid D}}{F_{D \mid D} + F_{A \mid D}} \quad (1)$$

The stoichiometry S is:

$$S = \frac{F_{D \mid D} + F_{A \mid D}}{F_{D \mid D} + F_{A \mid D} + F_{A \mid A}} \quad (2)$$

The FRET efficiency for a single donor acceptor distance R_{DA} is:

$$E = \frac{1}{1 + R_{DA}^6 / R_0^6} \quad (3)$$

The mean FRET efficiency for a discrete distribution of donor acceptor distances with the position vectors $\boldsymbol{R}_{D(i)}$ and $\boldsymbol{R}_{A(j)}$:

$$\langle E \rangle = \frac{1}{nm} \sum_{i=1}^{n} \sum_{j=1}^{m} \frac{1}{1 + \left| \boldsymbol{R}_{A(j)} - \boldsymbol{R}_{D(i)} \right|^6 / R_0^6} \quad (4)$$

The apparent donor acceptor distance $R_{\langle E \rangle}$ is computed from the average FRET efficiency for a distance distribution. It is a FRET-averaged quantity which was also referred to as FRET-averaged distance $\langle R_{DA} \rangle_E$ (ref [37]):

$$R_{\langle E \rangle} \equiv R(\langle E \rangle) = R_0 (\langle E \rangle^{-1} - 1)^{1/6} \quad (5)$$

Distance between the mean dye positions with the position vectors $\langle \boldsymbol{R}_{D(i)} \rangle$ and $\langle \boldsymbol{R}_{A(j)} \rangle$ obtained by normalized sums over all positions within the respective AVs:

$$R_{MP} = \left| \langle \boldsymbol{R}_{D(i)} \rangle - \langle \boldsymbol{R}_{A(j)} \rangle \right| = \left| \frac{1}{n} \sum_{i=1}^{n} \boldsymbol{R}_{D(i)} - \frac{1}{m} \sum_{j=1}^{m} \boldsymbol{R}_{A(j)} \right| \quad (6)$$

Further, the following subscripts and superscripts are used:

D or A: Concerning donor or acceptor

A/*D:* Acceptor fluorescence given donor excitation, *D*/*D, A*/*A* accordingly

Aem/*Dex:* Intensity in the acceptor channel given donor excitation, *Dem*/*Dex*, *Aem*/*Aex*, accordingly

app: apparent, i.e. including systematic, experimental offsets

BG: Background

DO/*AO :* Donor-only species/Acceptor-only species

DA: FRET species

i–iii: Indicates (i) the uncorrected intensity; (ii) intensity after BG correction; (iii) intensity after BG, alpha and delta corrections

The four correction factors are given by:

Leakage of D fluorescence into A channel:

$$\alpha = \frac{g_{R \mid D}}{g_{G \mid D}} = \frac{\langle {}^{ii}E_{app}^{(DO)} \rangle}{1 - \langle {}^{ii}E_{app}^{(DO)} \rangle}$$

Normalization of excitation intensities, *I,* and cross-sections, σ of A and D

$$\beta = \frac{\sigma_{A/R}}{\sigma_{D/G}} \frac{I_{Aex}}{I_{Dex}}$$

Normalization of effective fluorescence quantum yields, ${}^{eff}\Phi_F = a_b \cdot \Phi_F$, and detection efficiencies, *g,* of A and D. a_b is the fraction of molecules in the bright state and Φ_F is the fluorescence quantum yield without photophysical (saturation) effects.

$$\gamma = \frac{g_{R \mid A}}{g_{G \mid D}} \frac{{}^{eff}\Phi_{F,A}}{{}^{eff}\Phi_{F,D}}$$

Direct acceptor excitation by the donor excitation laser (lower wavelength)

$$\delta = \frac{\sigma_{A \mid G}}{\sigma_{A \mid R}} \frac{I_{Dex}}{\sigma_{Aex}} = \frac{\langle {}^{ii}S_{app}^{(AO)} \rangle}{1 - \langle {}^{ii}S_{app}^{(AO)} \rangle}$$

Here, we use the following definitions:

I: Experimentally observed intensity

F: Corrected fluorescence intensity

τ*:* Fluorescence lifetime [ns]

$\Phi_{F,A}$ or $\Phi_{F,D}$: Fluorescence quantum yield of A and D, respectively

r: Fluorescence anisotropy

R: Inter-dye distance [Å]

$g_{R/A}$ or $g_{G/D}$: Detection efficiency of the red detector (R) if only acceptor was excited or green detector (G) if donor was excited. Analogous for others.

$\sigma_{A/G}$: Excitation cross-section for acceptor when excited with green laser. Analogous for the others.

The Förster radius [Å], for a given J in units below is given by:

$$\frac{R_0}{\text{Å}} = 0.1208\sqrt[6]{\left(\frac{\Phi_{F,D}\kappa^2}{n_{im}^4}\right)\frac{J}{M^{-1}cm^{-1}nm^4}} \quad (7)$$

With the dipole orientation factor: $\kappa^2 = (\cos\theta_{AD} - 3\cos\theta_D \cos\theta_A)^2$

and the spectral overlap integral [$cm^{-1}M^{-1}nm^4$]:

$$J = \int_0^\infty \bar{F}_D(\lambda)\varepsilon_A(\lambda)\lambda^4 d\lambda$$

With the normalized spectral radiant intensity of the excited donor [nm^{-1}], defined as the derivative of the emission intensity F with respect to the wavelength:

$$\bar{F}_D(\lambda) \text{ with } \int_0^\infty \bar{F}_D(\lambda)\, d\lambda = 1$$

and the extinction coefficient of A [$M^{-1}\ cm^{-1}$]: $\varepsilon_A(\lambda)$

and the refractive index of the medium in-between the dyes: n_{im}

2 Samples

Altogether, 8 different FRET-samples were designed with the acceptor dyes positioned 15 or 23 base pairs away from the donor dyes. The exact sequences and dye positions are given in Supplementary Table 1 and Supplementary Note 1. We ordered them from IBA GmbH (Göttingen), which synthesized and labeled the single DNA strands followed by HPLC purification. Here the dyes were attached to a thymidine (dT), which is known to cause the least fluorescence quenching of all nucleotides[26].

Most labs measured the following four DNA samples listed in Supplementary Table 1. Therefore, we focus on these four samples in the main text of this manuscript. The additional samples and the corresponding measurements can be found in Supplementary Note 1 and Supplementary Figure 2 and Supplementary Table 4. The following buffer was

requested for all measurements: 20 mM $MgCl_2$, 5 mM NaCl, 5 mM Tris, at pH 7.5, degassing just before the measurement at room temperature.

The linker lengths were chosen in a way that all dyes had about the same number of flexible bonds between the dipole axis and the DNA. The Atto550, Alexa647 and Atto647N already have an intrinsic flexible part before the C-linker starts (Supplementary Figure 1). In addition, the DNAs were designed such that the distance ratio between the high FRET efficiency and low FRET efficiency sample should be the same for all samples, largely independent of R_0.

3 General correction procedure

The FRET efficiency E and Stoichiometry S are defined in eq.1 and eq.2. Determination of the corrected FRET E and S is largely based on the Lee et al. approach [17] and consists of the following steps: (1) data acquisition; (2) generation of uncorrected E vs. S 2D histograms; (3) background subtraction; (4) correction for the position-specific excitation in TIRF experiment; (5) correction for leakage and direct acceptor excitation; (6) correction for excitation intensities and absorption cross-sections, quantum yields and detection efficiencies.

3.1 Data acquisition—The sample with both dyes is measured and the three intensity time traces are extracted: acceptor emission upon donor excitation ($I_{Aem|Dex}$), donor-emission upon donor excitation ($I_{Dem|Dex}$), and acceptor-emission upon acceptor excitation ($I_{Aem|Aex}$).

For the confocal setups a straightforward burst identification is performed by binning the trace into 1 ms bins. Usually a minimum threshold (e.g. 50 photons) is applied to the sum of the donor and acceptor signals upon donor excitation for each bin. This threshold is used again in every step, such that the number of utilized bursts may change from step to step (if the γ correction factor is not equal to one). Some labs use sophisticated burst-search algorithms. For example, the dual channel burst search[38,39] recognizes the potential bleaching of each dye within bursts. Note that the choice of the burst-search algorithm can have an influence on the γ correction factor. For standard applications, the simple binning method is often sufficient, especially for well-characterized dyes and low laser powers. This study shows that the results do not significantly depend on these conditions (if applied properly), as every lab used its own setup and procedure at this stage. The number of photon bursts per measurement was typically between 1,000 and 10,000.

For the TIRF setups, traces with one acceptor and one donor are selected, defined by a bleaching step. In addition, only the relevant *range* of each trajectory – i.e. prior to photobleaching of either dye - is included in all further steps. The mean length of the time traces analyzed by the reference lab was 47 frames (18.8s) for the 185 traces of sample 1-lo and 15 frames (6s) for the 124 traces of sample 2-lo measured at an ALEX sampling rate of 2.5 Hz. For sample 1 bleaching was donor-limited, while bleaching for sample 2 was acceptor-limited, which explains the significant difference in frame lengths. For details on the analysis of the reference lab see ref [40].

3.2 2D histogram—A 2D histogram (Figure 2a,e) of the apparent stoichiometry, ${}^{i}S_{app}$, vs. apparent FRET efficiency, ${}^{i}E_{app}$, defined by Equations 8 and 9 is generated, where

$${}^{i}S_{app} = (I_{Aem\,|\,Dex} + I_{Dem\,|\,Dex})/(I_{Aem\,|\,Dex} + I_{Dem\,|\,Dex} + I_{Aem\,|\,Aex}) \quad (8)$$

$${}^{i}E_{app} = I_{Aem\,|\,Dex}/(I_{Aem\,|\,Dex} + I_{Dem\,|\,Dex}) \quad (9)$$

3.3 Background correction—Background $I^{(BG)}$ is removed from each uncorrected intensity ${}^{i}I$ separately, leading to the background corrected intensities ${}^{ii}I$, ${}^{ii}S_{app}$, ${}^{ii}E_{app}$:

$$\begin{aligned} {}^{ii}I_{Dem/Dex} &= {}^{i}I_{Dem/Dex} - I^{(BG)}_{Dem\,|\,Dex} \quad (10)\\ {}^{ii}I_{Aem/Aex} &= {}^{i}I_{Aem/Aex} - I^{(BG)}_{Aem\,|\,Aex}\\ {}^{ii}I_{Aem/Dex} &= {}^{i}I_{Aem/Dex} - I^{(BG)}_{Aem\,|\,Dex} \end{aligned}$$

For confocal measurements, the background is determined by averaging the photon count rate for all time bins that are below a threshold, which is e.g. defined by the maximum in the frequency vs. intensity plot (density of bursts should not be too high). Note, that a previous measurement of only the buffer can uncover potential fluorescent contaminants, but it can differ significantly from the background of the actual measurement. The background intensity is then subtracted from the intensity of each burst in each channel (eq. 10). Typical background values are 0.5–1 photon / ms (Figure 2b).

For TIRF measurements, various trace-wise or global background corrections can be applied. The most common method defines background as the individual offset (time average) after photobleaching of both dyes in each trace. Another possibility is to select the darkest spots in the illuminated area and to subtract an average background time trace from the data or to use a local background, e.g. with a mask around the particle. The latter two have the advantage that possible (exponential) background bleaching is also corrected. We have not investigated the influence of the kind of background correction during this study, but a recent study has shown that not all background estimators are suitable for samples with a high molecule surface coverage [41].

Overall, a correction of the background is very important, but can be done very well in different ways.

3.4 The position specific excitation correction (optional for TIRF)—The concurrent excitation profiles of both lasers are key for accurate measurements (see Supplementary Figure 5). Experimental variations across the field of view are accounted for using a position-specific normalization:

$$ {}^{ii}_{(\text{profile})}I_{Aem/Aex} = {}^{ii}I_{Aem/Aex}\frac{I_D(x', y')}{I_A(x, y)} \quad (11) $$

where $I_D(x', y')$ and $I_A(x, y)$ denote the excitation intensities at corresponding positions in the donor or acceptor image, respectively. Individual excitation profiles are determined as the mean image of a stack of images recorded while moving across a sample chamber with dense dye coverage.

3.5 Leakage (α) and direct excitation (δ)—After the background correction, the leakage fraction of the donor emission into the acceptor detection channel and the fraction of the direct excitation of the acceptor by the donor-excitation laser are determined. The correction factor for leakage (α) is determined by eq. 12 using the FRET efficiency of the donor-only population (D-only in Figure 2b,f). The correction factor for direct excitation (β) is determined by eq. 13 from the stoichiometry of the acceptor-only population (A-only in Figure 2b,f).

$$ \alpha = \frac{\langle {}^{ii}E_{app}^{(DO)} \rangle}{1 - \langle {}^{ii}E_{app}^{(DO)} \rangle} \quad (12) $$

$$ \delta = \frac{\langle {}^{ii}S_{app}^{(AO)} \rangle}{1 - \langle {}^{ii}S_{app}^{(AO)} \rangle} \quad (13) $$

where ${}^{ii}E_{app}^{(DO)}$ and ${}^{ii}S_{app}^{(AO)}$ are calculated from the background-corrected intensities ${}^{ii}I$ of the corresponding population, i.e. donor-only or acceptor-only, respectively. This correction together with the previous background correction results in the donor-only population being located at $\langle E \rangle = 0$, $\langle S \rangle = 1$ and acceptor-only population at $\langle S \rangle = 0$, $\langle E \rangle = 0...1$. The corrected acceptor fluorescence after donor excitation $F_{A|D}$ is given by eq. 14, which yields the updated expressions for the FRET efficiency and stoichiometry, eq. 15 and 16, respectively.

$$ F_{A \mid D} = {}^{ii}I_{Aem/Dex} - \alpha\, {}^{ii}I_{Dem/Dex} - \delta\, {}^{ii}I_{Aem/Aex} \quad (14) $$

$$ {}^{iii}E_{app} = F_{A \mid D}/(F_{A \mid D} + {}^{ii}I_{Dem/Dex}) \quad (15) $$

$$^{iii}S_{app} = (F_{A\mid D} + {}^{ii}I_{Dem/Dex})/(F_{A\mid D} + {}^{ii}I_{Dem/Dex} + {}^{ii}I_{Aem/Aex}) \quad (16)$$

In principle, the leaked donor signal could be added back to the donor emission channel[42]. However, this requires precise knowledge about spectral detection efficiencies, which is not otherwise required, and has no effect on the final accuracy of the measurement. As the determination of α and δ influences the γ and β correction in the next step, both correction steps can be repeated in an iterative manner if required (e.g. if the γ and β factors deviate largely from one).

3.6 γ and β correction factors—Differences in the excitation intensities and cross-section, as well as, quantum yields and detection efficiencies are accounted for by using the correction factors γ and β, respectively. If the fluorescence quantum yields do not depend on efficiencies or such dependence is negligible (*homogenous approximation*), mean values of efficiencies $\langle {}^{iii}E_{app}^{(DA)} \rangle$ and of stoichiometries $\langle {}^{iii}S_{app}^{(DA)} \rangle$ are related by eq. 17:

$$\langle {}^{iii}S_{app}^{(DA)} \rangle = \left(1 + \gamma\beta + (1-\gamma)\beta \langle {}^{iii}E_{app}^{(DA)} \rangle\right)^{-1} \quad (17)$$

So, in the homogeneous approximation, γ and β correction factors can be determined by fitting FRET populations to the ${}^{iii}S_{app}^{(DA)}$ *vs.* ${}^{iii}E_{app}^{(DA)}$ histogram with the line defined by eq. 17. As this method relies on the analysis of ${}^{iii}S_{app}^{(DA)}$, ${}^{iii}E_{app}^{(DA)}$ values obtained from multiple species, we term this method, *global* γ-correction. Such a fit can be performed for all FRET populations together, for any of their subsets, and in principle, for each single-species population separately (see below). Alternatively, a linear fit of inverse $\langle {}^{iii}S_{app}^{(DA)} \rangle$ *vs.* $\langle {}^{iii}E_{app}^{(DA)} \rangle$ with y-intercept a and slope b can be performed.

In this case, $\beta = a + b - 1$ and $\gamma = (a-1)/(a+b-1)$.

Error propagation, however, is more straightforward if eq. 17 is used. If there is a complex dependence between properties of dyes and efficiencies, the homogeneous approximation is no longer applicable. In this case, the relationship between ${}^{iii}S_{app}^{(DA)}$, ${}^{iii}E_{app}^{(DA)}$ for different populations (or even subpopulations for the same single-species) cannot be described by eq. 17 with a single γ correction factor. Here, β and γ can be determined for a single species. We call this "*single-species* γ*-correction*". This works only if the efficiency broadening is dominated by distance fluctuations. The reason for this assumption is the dependency of these correction factors on both the stoichiometry and the distance-dependent efficiency. In our study, global and local γ-correction yielded similar results. Therefore, the homogenous approximation, with distance fluctuations as the main cause for efficiency broadening, can be assumed for sample 1 and 2. Systematic variation of the γ-correction factor yields an error of about 10%.

Alternatively, determination of γ, β factors can be done trace-wise, e.g. as in msALEX experiments[43] where the γ factor is determined as the ratio of the decrease in acceptor signal and the increase in donor signal upon acceptor bleaching. We call such an alternative correction, *individual* γ-correction[15]. The analysis of local distributions can provide valuable insights about properties of the studied system.

After γ and β correction, the corrected donor (acceptor) fluorescence after donor (acceptor) excitation $F_{D|D}$ ($F_{A|A}$) amounts to:

$$F_{D\,|\,D} = \gamma\,{}^{ii}I_{Dem/Dex} \quad (18)$$

$$F_{A\,|\,A} = \frac{1}{\beta}\,{}^{ii}I_{Aem/Aex} \quad (19)$$

3.7 Fully corrected values—Application of all corrections leads to the estimates of real FRET efficiencies, E, and stoichiometries, S, from the background corrected intensities, ${}^{ii}I$. The explicit expressions of fully corrected FRET efficiency and stoichiometry are:

$$E = \frac{\left[{}^{ii}I_{Aem/Dex} - \alpha\,{}^{ii}I_{Dem/Dex} - \delta\,{}^{ii}I_{Aem/Aex}\right]}{\gamma[{}^{ii}I_{Dem/Dex}] + [{}^{ii}I_{Aem/Dex} - \alpha\,{}^{ii}I_{Dem/Dex} - \delta\,{}^{ii}I_{Aem/Aex}]} \quad (20)$$

$$S = \frac{\gamma\left[{}^{ii}I_{Dem/Dex}\right] + \left[{}^{ii}I_{Aem/Dex} - \alpha\,{}^{ii}I_{Dem/Dex} - \delta\,{}^{ii}I_{Aem/Aex}\right]}{\gamma[{}^{ii}I_{Dem/Dex}] + [{}^{ii}I_{Aem/Dex} - \alpha\,{}^{ii}I_{Dem/Dex} - \delta\,{}^{ii}I_{Aem/Aex}] + {}^{1}\!/\!_{\beta}[{}^{ii}I_{Aem/Aex}]} \quad (21)$$

Plots of the E vs. S histogram are shown in Figure 2d and 2h. Now, the FRET population should be symmetric to the $S = 0.5$ line. The donor-only population should still be located at $E = 0$ and the acceptor-only population at $S = 0$. Finally, the corrected FRET efficiency histogram is generated using events with a stoichiometry of $0.3 < S < 0.7$ (see Figure 2 histograms). The expected value of the corrected FRET efficiencies $\langle E \rangle$ is deduced as the center of a Gaussian fit to the efficiency histogram. This is a good approximation for FRET efficiencies in the range between about 0.1 and 0.9. In theory, the shot-noise limited efficiencies follow a binomial distribution if the photon number per burst is constant. For extreme efficiencies or data with a small average number of photons per burst, the efficiency distribution can no longer be approximated with a Gaussian. In this case and also in the case of efficiency broadening due to distance fluctuations, a detailed analysis of the photon statistics can be useful [38,44–46].

4 Uncertainty in distance due to R_0

According to Förster theory[1], the FRET efficiency, E, and the distance, R, are related by eq. 3. In this study, we focused on comparing E in a blind study across different labs. The Seidel lab determined an R_0 for this system to convert efficiencies to distances. There are many excellent reviews on how to determine the Förster radius R_0 [16,47,48] and a complete discussion would be beyond the scope of this experimental comparison study. In the following, we estimate and discuss the different sources of uncertainty in R_0, by utilizing standard error propagation (see also Supplementary Note 6 *and ref* [26]). R_0 is given by eq. 7.

The 6th power of the Förster radius is proportional to the relative dipole orientation factor κ^2, the donor quantum yield $\Phi_{F,D}$, the overlap integral J, as well as n^{-4}, where n is the refractive index of the medium:

$$R_0^6 \sim \kappa^2 \cdot \Phi_{F,D} \cdot J \cdot n^{-4} \quad (22)$$

For Figure 5b, we use a total Förster radius related distance uncertainty of 7 %, which is justified by the following estimate. Please note that the error in the dipole orientation factor is always very specific for the investigated system, while the errors in the donor quantum yield, overlap integral and refractive index are more general, but their mean values do also depend on the environment.

4.1 The refractive index—Different values for the refractive index in FRET systems have been used historically, but ideally the refractive index of the donor-acceptor intervening medium n_{im} should be used, though some experimental studies suggest that the use of the refractive index of the solvent may be appropriate, but this is still open for discussion (see e. g. discussion in[49]).

$$R_0^6(n) \sim n_{im}^{-4} \quad (23)$$

In the worst case, this value n_{im} might be anywhere in-between the refractive index of the solvent (n_{water} = 1.33) and a refractive index for the dissolved molecule ($n < n_{oil}$=1.52) [50], i.e. $n_{water} < n_{im} < n_{oil}$. This would result in a maximum uncertainty of $\Delta n_{im} < 0.085$. As recommended by Clegg, we used n_{im} = 1.40 to minimize this uncertainty[51] (see Supplementary Table 6). The distance uncertainty propagated from the uncertainty of the refractive indices can then be assumed to be:

$$\Delta R_0(n) \approx \frac{4}{6} R_o \frac{\Delta n_{im}}{n} < 0.04 \cdot R_0 \quad (24)$$

4.2—The donor quantum yield $\Phi_{F,D}$ is position dependent, therefore we measured the fluoresence lifetimes and quantum yields of the free dye Atto550 and the 1-hi, 1-mid and 1-lo donor only labeled samples (see Supplementary Table 2).

In agreement with Sindbert et al. [37], the uncertainty of the quantum yield is estimated at $\Delta\Phi'_{F,} = 5$ % arising from the uncertainties of the Φ_F values reference dyes and the precision of the absorption and fluorescence measurements. Thus, the distance uncertainty owing to the quantum yield is estimated at:

$$\Delta R_0(\Phi_{F,D}) \approx \frac{R_0}{6}\frac{\Delta\Phi_{F,D}}{\Phi_{F,D}} = 0.01 \cdot R_0 \quad (25)$$

4.3—The overlap integral *J* was measured for the unbound dyes in solution (Atto550 and Atto647N), as well as for samples 1-lo and 1-mid. This resulted in a deviation of about 10 % for J using the literature values for the extinction coefficients. All single stranded labeled DNA samples used in this study were purified with HPLC columns providing a labeling efficiency of at least 95 %. The label efficiencies of the single stranded singly-labeled DNA and of the double stranded singly-labeled DNA samples were determined by the ratio of the absorption maxima of the dye and the DNA and were all above 97 %. This indicates an error of the assumed exctinction coefficient of less than 3 %. Thus, the distance uncertainty due to the overlap spectra and a correct absolute acceptor extinction coefficient can be estimated by eq. 26. However, the uncertainty in the acceptor extinction coefficient might be larger for other environments, such as when bound to a protein.

$$\Delta R_0(\mathrm{J}) \approx \frac{R_0}{6}\frac{\Delta \mathrm{J}}{\mathrm{J}} = 0.025 \cdot R_0 \quad (26)$$

In addition to the above uncertainty estimation, the ***J*****-**related uncertainty can also be obtained by verifying the self-concistency of a β-factor network [9]. Finally, we found little uncertainty by using the well-tested dye Atto647N. Fluorescence spectra were measured on a Fluoromax4 spectrafluorimeter (Horiba, Germany). Absorbance spectra were recorded on a Cary5000 UV/VIS spectrometer (Agilent, USA). See Supplementary Figure 6.

4.4 The κ^2 factor and model assumptions—The uncertainty in the distance depends on the dye model used [22]. Several factors need to be considered, given the model assumptions of unrestricted dye rotation, equal sampling of the entire accessible volume, and the following rate inequality $k_{rot} \gg k_{FRET} \gg k_{diff} \gg k_{int}$.

First, the use of $\langle \kappa^2 \rangle = 2/3$ is justified if $k_{rot} \gg k_{FRET}$, because then there is rotational averaging of the dipole orientation during energy transfer. k_{rot} is determined from the rotational correlation time $\rho_1 < 1$ ns and k_{FRET} is determined from the fluorescence lifetimes 1 ns < τ_{fl} < 5 ns. Hence the condition $k_{rot} \gg k_{FRET}$ is not strictly fulfilled. We estimate the error this introduces into κ^2 from the time-resolved anisotropies of donor and acceptor dyes. If the transfer rate is smaller than the fast component of the anisotropy decay (rotational correlation time) of donor and acceptor. Then, the combined anisotropy, $r_{G,}$ is given by the residual donor and acceptor anisotropies ($r_{D,\infty}$ and $r_{A,\infty}$, respectively):

$$r_C = \sqrt{r_{A,\infty}}\sqrt{r_{D,\infty}} \quad (27)$$

In theory, the donor and the acceptor anisotropy should be determined at the time of energy transfer. If the transfer rate is much slower than the fast component of the anisotropy decay of donor and acceptor, the residual anisotropy can be used (Supplementary Figure 7)[9]. Also, the steady state anisotropy values can give an indication of the rotational freedom of the dyes on the relevant time scales, if the inherent effect by the fluorescence lifetimes is taken into account (see Perrin equation, Supplementary Table 2 and Supplementary Figure 8).

If the steady-state anisotropy and r_C are low (< 0.2), one can assume (but not prove) sufficient isotropic coupling (rotational averaging), i.e. $\langle \kappa^2 \rangle$ = 2/3, with an uncertainty of about 5 %[9]:

$$\Delta R_0(\kappa^2, r_C < 0.2) \approx 0.05 \cdot R_0 \quad (28)$$

4.5 Spatial sampling—In addition, it is assumed that both dyes remain in a fixed location for the duration of the donor lifetime, i.e. $k_{FRET} \gg k_{diff}$: where k_{diff} is defined as the inverse of the diffusion time through the complete AV. Recently the diffusion coefficient for a tethered Alexa488 dye was determined to be D=10 Å^2/ns (ref. [30]). Therefore, k_{diff} is smaller than the k_{FRET}. For short distances (< 5 Å) the rates become comparable, but the effect on the inter dye distance distribution within the donor lifetime is small, as has been observed in time-resolved experiments. We also assumed that, in the experiment, the efficiencies are averaged for all possible inter-dye positions. This is the case when $k_{\mathrm{diff}} \gg k_{\mathrm{int}}$, which is a very good assumption for TIRF experiment with k_{int} > 100 ms and also for confocal experiments with k_{int} around 1 ms.

4.6 Overall uncertainty in R_0—Time-resolved anisotropy measurements of samples 1 and 2 resulted in combined anisotropies below 0.1. Therefore we assumed isotropic coupling to obtain R_{MP}. The R_{MP} match the model distances very well, further supporting these assumptions. Finally, an experimental study on κ^2 distributions also obtained typical errors of 5 %[37].

The overall uncertainty for the Förster radius would then result in:

$$\Delta R_0(n^{-4}, \Phi_{F,D}, J, \kappa^2) = \sqrt{\Delta R_0(n)^2 + \Delta R_0(\varnothing_{F,D})^2 + \Delta R_0(J)^2 + \Delta R_0(\kappa^2)^2} \lesssim 0.07 \cdot R_0 \quad (29)$$

The absolute values determined for this study are summarized in Supplementary Table 6. Please note that the photophysical properties of dyes vary in different buffers and when attached to different biomolecules. Therefore, all four quantities contributing to the uncertainty in R_0 should be measured for the system under investigation. When supplier

values or values from other studies are applied, the uncertainty can be much larger. The values specified here could be further evaluated and tested in another blind study.

4.7 Comparing distinct dye pairs—Even though time-resolved fluorescence anisotropy can monitor whether dye rotation is fast, the possibility of dyes interacting with the DNA cannot be fully excluded. Thus, it is not clear if the dye molecule is completely free to sample the computed AV (free diffusion), or whether there are sites of attraction (preferred regions) or sites of repulsion (disallowed regions). In order to validate the model assumption of a freely rotating and diffusing dye we define the ratio, R_{rel}, for two apparent distances measured with the same dye pair (e.g. when comparing the lo- to the mid-distance):

$$R_{rel} = \frac{R_{\langle E\rangle, lo}}{R_{\langle E\rangle, mid}} = \frac{R_{0,lo}}{R_{0,mid}} \sqrt[6]{\frac{1/E_{lo} - 1}{1/E_{mid} - 1}} = \sqrt[6]{\frac{\kappa^2_{lo} \Phi_{D,lo} J_{lo} n^4_{mid}}{\kappa^2_{mid} \Phi_{D,mid} J_{mid} n^4_{lo}}} \sqrt[6]{\frac{1/E_{lo} - 1}{1/E_{mid} - 1}} = f \cdot \sqrt[6]{\frac{1/E_{lo} - 1}{1/E_{mid} - 1}} \quad (30)$$

For comparing the other apparent distances the ratio is adapted accordingly. Computed values relative to the mid-distance are shown in Supplementary Table 4. Note that R_{rel} are (quasi) independent of R_0 for the following reasons: First, the donor positions are identical for all lo-,mid- and hi-samples, respectively. Therefore, the following assumptions can be made: (i) the ratio of the donor quantum yields are identical; (ii) the ratio of the spectral overlaps J for the lo-,mid- and hi- samples of one and the same dye pair should be the same; (iii) for the given geometry (see Figure 1) the refractive indices n_{im} of the medium between the dyes should also be very similar; (iv) the ratio of the orientation factors κ^2 should be nearly equal as the measured donor anisotropies are low for the lo-,mid- and hi- positions. Second, the acceptor extinction coefficients eliminate each other as the acceptor is at the same position for the lo-,mid- and hi-samples. Thus, the different dye pairs and the model used in this study should all give similar values for R_{rel}. Therefore we compared the R_{rel} values for different dye pairs to judge whether for a particular dye pair the model assumptions are in agreement with the experimental data. Given our relative error in the determined distance of maximal 2.8% (Figure 5a) this is actually the case for all dye pairs investigated.

Supplementary Material

Refer to Web version on PubMed Central for supplementary material.

Authors

Björn Hellenkamp[1a,b,°], Sonja Schmid[1a,c,°], Olga Doroshenko[20], Oleg Opanasyuk[20], Ralf Kühnemuth[20], Soheila Rezaei Adariani[15], Benjamin Ambrose[2], Mikayel Aznauryan[9], Anders Barth[21], Victoria Birkedal[9], Mark E. Bowen[11], Hongtao Chen[26], Thorben Cordes[14,25], Tobias Eilert[19], Carel Fijen[7], Christian Gebhardt[25], Markus Götz[1a], Giorgos Gouridis[14,25], Enrico Gratton[26], Taekjip Ha[22], Pengyu Hao[12],

Christian A. Hanke[20], Andreas Hartmann[17], Jelle Hendrix[5,6], Lasse L. Hildebrandt[9], Verena Hirschfeld[16], Johannes Hohlbein[7,8], Boyang Hua[22], Christian G. Hübner[16], Eleni Kallis[19], Achillefs N. Kapanidis[10], Jae-Yeol Kim[23], Georg Krainer[17,18], Don C. Lamb[21], Nam Ki Lee[23], Edward A. Lemke[3a,b,c], Brié Levesque[11], Marcia Levitus[24], James J. McCann[11], Nikolaus Naredi-Rainer[21], Daniel Nettels[4], Thuy Ngo[22], Ruoyi Qiu[12], Nicole C. Robb[10], Carlheinz Röcker[19], Hugo Sanabria[15], Michael Schlierf[17], Tim Schröder[27], Benjamin Schuler[4], Henning Seidel[16], Lisa Streit[19], Johann Thurn[1a], Philip Tinnefeld[13,27], Swati Tyagi[3c], Niels Vandenberk[5], Andrés Manuel Vera[27], Keith R. Weninger[12], Bettina Wünsch[13], Inna S. Yanez-Orozco[15], Jens Michaelis[19,*], Claus A.M. Seidel[20,*], Timothy D. Craggs[2,10,*], and Thorsten Hugel[1a,d,*]

Affiliations

[1a]Institute of Physical Chemistry, University of Freiburg, Germany [1b]Engineering and Applied Sciences, Columbia University, USA [1c]Department of Bionanoscience, Kavli Institute of Nanoscience Delft, Delft University of Technology, The Netherlands [1d]BIOSS Centre for Biological Signalling Studies, University of Freiburg [2]Department of Chemistry, University of Sheffield, S3 7HF, UK [3a]Departments of Biology and Chemistry, Pharmacy and Geosciences, Johannes Gutenberg-University Mainz, Johannes-von-Mullerweg 6, 55128 Mainz, Germany [3b]Institute of Molecular Biology (IMB), Ackermannweg 4, 55128 Mainz, Germany [3c]Structural and Computational Biology Unit, European Molecular Biology Laboratory (EMBL), Meyerhofstrasse 1, 69117 Heidelberg, Germany [4]Department of Biochemistry, University of Zurich, Switzerland [5]Laboratory for Photochemistry and Spectroscopy, Department of Chemistry, University of Leuven, B-3001 Leuven, Belgium [6]Dynamic Bioimaging Lab, Advanced Optical Microscopy Center and Biomedical Research Institute, Hasselt University, Agoralaan C (BIOMED), B-3590 Hasselt, Belgium [7]Laboratory of Biophysics, Wageningen University & Research, 6708 WE, Wageningen, NL [8]Microspectroscopy Research Facility Wageningen, Wageningen University & Research, 6708 WE, Wageningen, NL [9]Interdisciplinary Nanoscience Center and Department of Chemistry, Aarhus University, 8000 Aarhus C, Denmark [10]Gene Machines group, Clarendon Laboratory, Department of Physics, University of Oxford, Parks Road, OX1 3PU, Oxford, UK [11]Department of Physiology & Biophysics, Stony Brook University, Stony Brook, NY 11794, USA [12]Department of Physics, North Carolina State University, Raleigh, NC 27695 USA [13]Institute of Physical & Theoretical Chemistry, and Braunschweig Integrated Centre of Systems Biology (BRICS), and Laboratory for Emerging Nanometrology (LENA), Braunschweig University of Technology, Rebenring 56, 38106 Braunschweig, Germany [14]Molecular Microscopy Research Group, Zernike Institute for Advanced Materials, University of Groningen, Nijenborgh 4, 9747 AG Groningen, The Netherlands [15]Department of Physics and Astronomy, Clemson University, 29634 Clemson, SC. USA [16]Institute of Physics, University of Lübeck, Germany [17]B CUBE – Center for Molecular Bioengineering, TU Dresden, Arnoldstr. 18, 01307 Dresden, Germany [18]Molecular Biophysics, Technische Universität Kaiserslautern (TUK), Erwin-Schrödinger-Str. 13, 67663 Kaiserslautern, Germany [19]Institute for

Biophysics, Ulm University, Albert-Einstein-Allee 11, 89081 Ulm, Germany [20]Molecular Physical Chemistry, Heinrich-Heine-Universität Düsseldorf, 40225 Düsseldorf, Germany [21]Physical Chemistry, Department of Chemistry, Nanosystems Initiative Munich, Center for Integrated Protein Science Munich (CiPSM) and Center for Nanoscience (CeNS), Ludwig-Maximilians-Universität München, 81377 Munich, Germany [22]Ha lab, Department of Biomedical Engineering, John Hopkins University, USA [23]School of Chemistry, Seoul National University, Seoul, South Korea [24]School of Molecular Sciences and The Biodesign Institute, Arizona State University, USA [25]Physical and Synthetic Biology, Faculty of Biology, Ludwig Maximilians-Universität München, Großhadernerstr. 2-4, 82152 Planegg-Martinsried, Germany [26]Department of Biomedical Engineering, University of California, Irvine, Irvine, California, USA [27]Department of Chemistry, Ludwig-Maximilians-Universitaet Muenchen, Butenandtstr. 5-13, 81377 München, Germany

Acknowledgments

We thank the William Eaton Lab for early measurements that helped to design this study. We thank T. Peulen, M. Dimura and R. McDonald for stimulating discussions on FRET measurements, data analysis and mode1ling, and B. Bulat for measuring fluorescence quantum yields of Atto550 and 1-mid (Atto550). We also thank the company Atto-Tec for providing a reference sample of the dye Atto550 for the fluorescence characterization. The authors acknowledge the networking support by the Dr. Wilhelm Heinrich und Else Heraeus Foundation and the COST Action CM1306 “Understanding Movement and Mechanism in Molecular Machines”. At the 512th WE-Heraeus-Seminar “Single molecule kinetics” (Bad Honnef, Germany, 2012) the idea of a worldwide benchmark study of standard FRET-rulers emerged and was further evolved during the international COST symposium “Integrating spectroscopic and theoretical methods to analyse molecular machines” (Castle of Ringberg, Germany, 2014).

Parts of this work were funded by the European Research Council through ERC grant agreement no. 261227 to A.N.K., no. 638536 to T.C., no. 671208 to C.A.M.S. and no. 681891 to T.H. J.M. acknowledges funding by the Deutsche Forschungsgemeinschaft (DFG) grant MI 749/4-1, P.T. by grant TI 329/10-1 and M.S. by grant SCHL 1896/3-1. B.S. acknowledges funding from the Swiss National Science Foundation. This work was supported by German Federal Ministry of Education and Research (BMBF) with 03Z2EN11 to M.S. J.H. acknowledges the Research Foundation Flanders (FWO) (grant G0B4915N). N.V. acknowledges the agency for Innovation by Science and Technology (IWT Flanders) for a doctoral scholarship. V.B. acknowledges funding from the Danish Council for Independent Research (Sapere Aude grant 0602-01670B) and the Novo Nordisk Foundation (NNF15OC0017956). A.N.K. was supported by the UK BBSRC grant BB/H01795X/1. M.B. was supported by the National Institute of Mental Health grant MH081923. H.S., S.R.A. and I.S.Y. acknowledge support from start-up funds from Clemson University. K.R.W. acknowledges NIH grants GM109832 and GM118508. T.H. was funded by an NIH grant GM 112659. H.S. acknowledges support by NSF Career MCS1749778. E.K. acknowledges the Carl-Zeiss-Stiftung for a doctoral fellowship. G.K. acknowledges the Stipendienstiftung Rheinland-Pfalz for support with a doctoral scholarship. B.W. acknowledges support by the Braunschweig International Graduate School of Metrology B-IGSM and the DFG Research Training Group GrK1952/1 “Metrology for Complex Nanosystems”. T.D.C. was supported by start-up funds from the University of Sheffield. N.K.L. acknowledges the National Research Foundation of Korea funded by the Ministry of Science and ICT (NRF-2017R1A2B3010309).

References

1. Förster T. Zwischenmolekulare Energiewanderung und Fluoreszenz. Ann Phys. 1948; 437:55–75.
2. Stryer L, Haugland RP. Energy Transfer: a Spectroscopic Ruler. Proc Natl Acad Sci U S A. 1967; 58:719–726. [PubMed: 5233469]
3. Murchie AI, et al. Fluorescence Energy Transfer Shows that the Four-Way DNA Junction is a Right-Handed Cross of Antiparallel Molecules. Nature. 1989; 341:763–766. [PubMed: 2797209]
4. Mekler V, et al. Structural Organization of Bacterial RNA Polymerase Holoenzyme and the RNA Polymerase-promoter Open Complex. Cell. 2002; 108:599–614. [PubMed: 11893332]

5. Ha T, et al. Probing the Interaction Between Two Single Molecules: Fluorescence Resonance Energy Transfer Between a Single Donor and a Single Acceptor. Proc Natl Acad Sci USA. 1996; 93:6264–6268. [PubMed: 8692803]
6. Schuler B, Lipman EA, Steinbach PJ, Kumke M, Eaton WA. Polyproline and the “Spectroscopic Ruler” Revisited with Single-Molecule Fluorescence. Proc Natl Acad Sci USA. 2005; 102:2754–2759. [PubMed: 15699337]
7. Choi UB, et al. Single-Molecule FRET-derived Model of the Synaptotagmin 1-SNARE Fusion Complex. Nat Struct Mol Biol. 2010; 17:318–U384. [PubMed: 20173763]
8. Kalinin S, et al. A toolkit and benchmark study for FRET-restrained high-precision structural modeling. Nat Meth. 2012; 9:1218–1227.
9. Hellenkamp B, Wortmann P, Kandzia F, Zacharias M, Hugel T. Multidomain Structure and Correlated Dynamics Determined by Self-Consistent FRET Networks. Nat Meth. 2017; 14:174–180.
10. Eilert T, Beckers M, Drechsler F, Michaelis J. Fast-NPS - A Markov chain Monte Carlo-based analysis tool to obtain structural information from single-molecule FRET measurements. Comput Phys Commun. 2017; 219:377–389.
11. Hofmann D, Korzdorfer T, Kummel S. Energy Transfer and Forster’s Dipole Coupling Approximation Investigated in a Real-Time Kohn-Sham Scheme. Phys Rev A. 2010; 82
12. Spiegel JD, Fulle S, Kleinschmidt M, Gohlke H, Marian CM. Failure of the IDA in FRET Systems at Close Inter-Dye Distances is Moderated by Frequent Low k(2) Values. J Phys Chem B. 2016; 120:8845–8862. [PubMed: 27490865]
13. Sakon JJ, Weninger KR. Detecting the conformation of individual proteins in live cells. Nat Meth. 2010; 7:203–205.
14. Sabanayagam CR, Eid JS, Meller A. Using Fluorescence Resonance Energy Transfer to Measure Distances Along Individual DNA Molecules: Corrections due to Nonideal Transfer. J Chem Phys. 2005; 122:61103–61107.
15. McCann JJ, Choi UB, Zheng L, Weninger K, Bowen ME. Optimizing Methods to Recover Absolute FRET Efficiency from Immobilized Single Molecules. Biophys J. 2010; 99:961–970. [PubMed: 20682275]
16. Sisamakis E, Valeri A, Kalinin S, Rothwell PJ, Seidel CAM. Accurate Single-Molecule FRET Studies Using Multiparameter Fluorescence Detection. Methods Enzymol. 2010; 475:455–514. [PubMed: 20627168]
17. Lee NK, et al. Accurate FRET Measurements Within Single Diffusing Biomolecules Using Alternating-Laser Excitation. Biophys J. 2005; 88:2939–2953. [PubMed: 15653725]
18. Kudryavtsev V, et al. Combining MFD and PIE for Accurate Single-Pair Förster Resonance Energy Transfer Measurements. ChemPhysChem. 2012; 13:1060–1078. [PubMed: 22383292]
19. Hohlbein J, Craggs TD, Cordes T. Alternating-Laser Excitation: Single-Molecule FRET and Beyond. Chem Soc Rev. 2014; 43:1156–1171. [PubMed: 24037326]
20. Margeat E, et al. Direct Observation of Abortive Initiation and Promoter Escape Within Single Immobilized Transcription Complexes. Biophys J. 2006; 90:1419–1431. [PubMed: 16299085]
21. Muschielok A, et al. A Nano-Positioning System for Macromolecular Structural Analysis. Nat Meth. 2008; 5:965–971.
22. Beckers M, Drechsler F, Eilert T, Nagy J, Michaelis J. Quantitative Structural Information from Single-Molecule FRET. Farad Discuss. 2015; 184:117–129.
23. Dimura M, et al. Quantitative FRET Studies and Integrative Modeling Unravel the Structure and Dynamics of Biomolecular Systems. Curr Opin Struct Biol. 2016; 40:163–185. [PubMed: 27939973]
24. Brunger AT, Strop P, Vrljic M, Chu S, Weninger KR. Three-Dimensional Molecular Modeling with Single Molecule FRET. J Struct Biol. 2011; 173:497–505. [PubMed: 20837146]
25. Craggs TD, , et al. Substrate conformational dynamics drive structure-specific recognition of gapped DNA by DNA polymerase. 2018.
26. Nagy J, Eilert T, Michaelis J. Precision and Accuracy in smFRET based structural studies - a benchmark study of the FAST-Nano-Positioning System. J Chem Phys. 2018:148.

27. Ivani I, et al. Parmbsc1: a refined force field for DNA simulations. Nat Meth. 2016; 13:55–58.
28. Neubauer H, et al. Orientational and dynamical heterogeneity of rhodamine 6G terminally attached to a DNA helix revealed by NMR and single-molecule fluorescence spectroscopy. J Am Chem Soc. 2007; 129:12746–12755. [PubMed: 17900110]
29. Iqbal A, et al. Orientation dependence in fluorescent energy transfer between Cy3 and Cy5 terminally attached to double-stranded nuclelic acids. Proc Natl Acad Sci USA. 2008; 105:11176–11181. [PubMed: 18676615]
30. Peulen TO, Opanasyuk O, Seidel CAM. Combining graphical and analytical methods with molecular simulations to analyze time-resolved FRET-measurements of labeled macromolecules accurately. J Phys Chem B. 2017; 121:8211–8241. [PubMed: 28709377]
31. Digman MA, Caiolfa VR, Zamai M, Gratton E. The Phasor approach to fluorescence lifetime imaging analysis. Biophys J. 2008; 84:L14–L16.
32. Kapanidis AN, et al. Fluorescence-aided molecule sorting: Analysis of structure and interactions by alternating-laser excitation of single molecules. Proc Natl Acad Sci USA. 2004; 101:8936–8941. [PubMed: 15175430]
33. Müller BK, Zaychikov E, Bräuchle C, Lamb DC. Pulsed interleaved excitation. Biophys J. 2005; 89:3508–3522. [PubMed: 16113120]
34. Wozniak AK, Schröder GF, Grubmüller H, Seidel CAM, Oesterhelt F. Single-Molecule FRET Measures Bends and Kinks in DNA. Proc Natl Acad Sci USA. 2008; 105:18337–18342. [PubMed: 19020079]
35. Stelzl LS, Erlenbach N, Heinz M, Prisner TF, Hummer G. Resolving the conformational dynamics of DNA with Ångström resolution by pulsed electron-electron double resonance and molecular dynamics. J Am Chem Soc. 2017; 139:11674–11677. [PubMed: 28777549]
36. Levitus M, Ranjit S. Cyanine dyes in biophysical research: the photophysics of polymethine fluorescent dyes in biomolecular environments. Q Rev Biophys. 2011; 44:123–151. [PubMed: 21108866]
37. Sindbert S, et al. Accurate Distance Determination of Nucleic Acids via Förster Resonance Energy Transfer: Implications of Dye Linker Length and Rigidity. J Am Chem Soc. 2011; 133:2463–2480. [PubMed: 21291253]
38. Nir E, et al. Shot-Noise Limited Single-Molecule FRET Histograms: Comparison Between Theory and Experiments. J Phys Chem B. 2006; 110:22103–22124. [PubMed: 17078646]
39. Barth A, Voith von Voithenberg L, DCL. Advanced Photon Counting: Applicatios, Methods, Instrumentation. Vol. 15. Springer; 2015. MFD-PIE and PIE-FI: Ways to Extract More Information with TCSPC; 129–157.
40. Schmid S, Hugel T. Efficient use of single molecule time traces to resolve kinetic rates, models and uncertainties. The Journal of Chemical Physics. 2018; 148
41. Preus S, Hildebrandt LL, Birkedal V. Optimal Background Estimators in Single-Molecule FRET Microscopy. Biophys J. 2016; 111:1278–1286. [PubMed: 27653486]
42. Neher R, Neher E. Optimizing Imaging Parameters for the Separation of Multiple Labels in a Fluorescence Image. Journal of Microscopy-Oxford. 2004; 213:46–62.
43. Hildebrandt LL, Preus S, Birkedal V. Quantitative Single Molecule FRET Efficiencies Using TIRF Microscopy. Farad Discuss. 2015; 184:131–142.
44. Deniz AA, et al. Single-Pair Fluorescence Resonance Energy Transfer on Freely Diffusing Molecules: Observation of Forster Distance Dependence and Subpopulations. Proc Natl Acad Sci USA. 1999; 96:3670–3675. [PubMed: 10097095]
45. Antonik M, Felekyan S, Gaiduk A, Seidel CAM. Separating Structural Heterogeneities from Stochastic Variations in Fluorescence Resonance Energy Transfer Distributions via Photon Distribution Analysis. J Phys Chem B. 2006; 110:6970–6978. [PubMed: 16571010]
46. Kalinin S, Valeri A, Antonik M, Felekyan S, Seidel CAM. Detection of Structural Dynamics by FRET: A Photon Distribution and Fluorescence Lifetime Analysis of Systems with Multiple States. J Phys Chem B. 2010; 114:7983–7995. [PubMed: 20486698]
47. Clegg RM. Förster Resonance Energy Transfer - FRET What Is It, Why Do It, And How It's Done. In: Gadella TWJ, editorLaboratory Techniques in Biochemistry and Molecular Biology. Vol. 33. Elsevier Science; 2009. 1–57.

48. Braslavsky SE, et al. Pitfalls and Limitations in the Practical Use of Förster's Theory of Resonance Energy Transfer. Photochem Photobiol Sci. 2008; 7:1444–1448. [PubMed: 19037495]

49. Knox RS, van Amerongen H. Refractive Index Dependence of the Forster Resonance Excitation Transfer Rate. J Phys Chem B. 2002; 106:5289–5293.

50. Voros J. The Density and Refractive Index of Adsorbing Protein Layers. Biophys J. 2004; 87:553–561. [PubMed: 15240488]

51. Clegg RM. Fluorescence Resonance Energy Transfer and Nucleic Acids. Methods Enzymol. 1992; 211:353–388. [PubMed: 1406315]

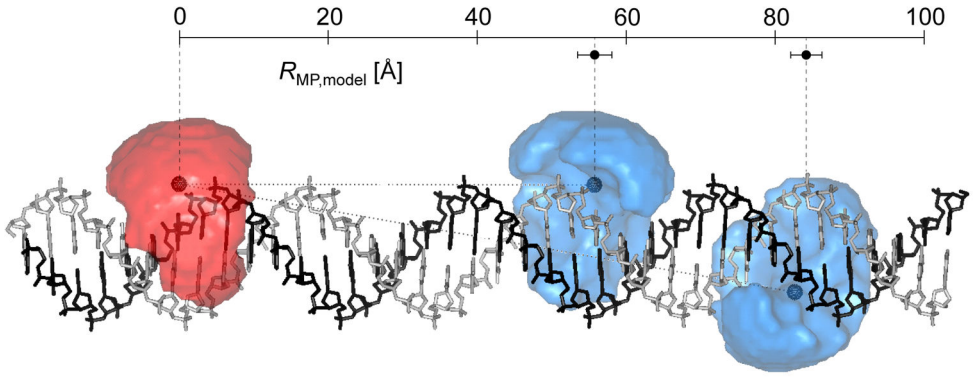

Fig. 1.

Schematic of the FRET standard molecules. Double-stranded DNA is labeled with a FRET pair at 15 or 23 base-pair separation for the “lo” and “mid” samples, respectively (for sequences see Online Methods). The accessible volumes (AVs) of the dyes (donor: blue; acceptor: red) are illustrated as semi-transparent surfaces and were calculated using freely available software [8]. The mean dye positions are indicated by darker spheres (assuming homogenously distributed dye positions, see Supplementary Note 3). The distance between the mean dye positions is defined as $R_{MP,model}$. Calculated values for $R_{MP,model}$ together with error bars obtained by varying parameters of the AV model are displayed (see Supplementary Note 3). The B-DNA model was generated using the Nucleic Acid Builder version 04/17/2017 for Amber [27].

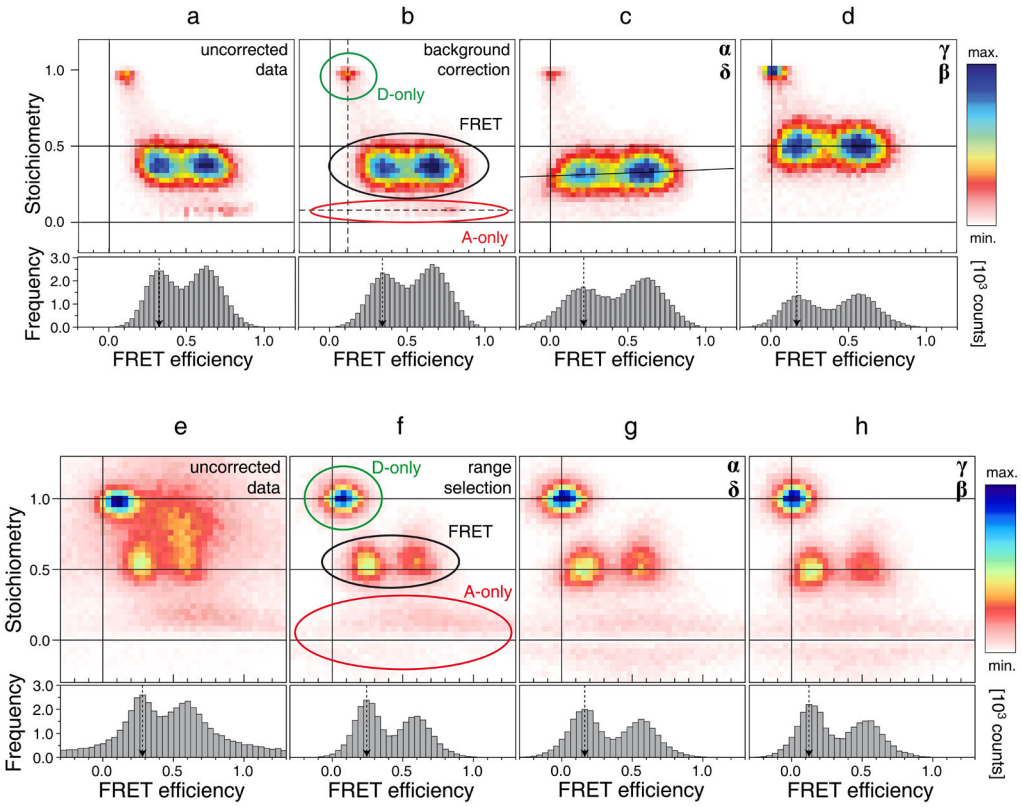

Fig. 2.

Stepwise data correction, shown for the combination of sample 1-lo and 1-mid. **(a)–(d)**: Workflow for correcting the confocal data: for background (a-->b), leakage (factor α) and direct excitation (δ)(b-->c), excitation and detection factors (β,γ)(c-->d). **(e)–(h)**: Workflow for correcting the TIRF data: for background and photobleaching by selection of the pre-bleached range (e-->f), leakage and direct excitation (f-->g), detection and excitation factors (g-->h). The efficiency histograms below show a projection of the data with a stoichiometry between 0.3 and 0.7. Note the significant shift of the FRET efficiency peak positions, especially for the low FRET efficiency peak (E~0.25 uncorrected to E~ 0.15 fully corrected).The general terms “stoichiometry” and “FRET efficiency” are used in place of the corresponding specific terms for each correction step (Online Methods section 3). Donor only (D-only), FRET and acceptor only (A-only) populations are specified.

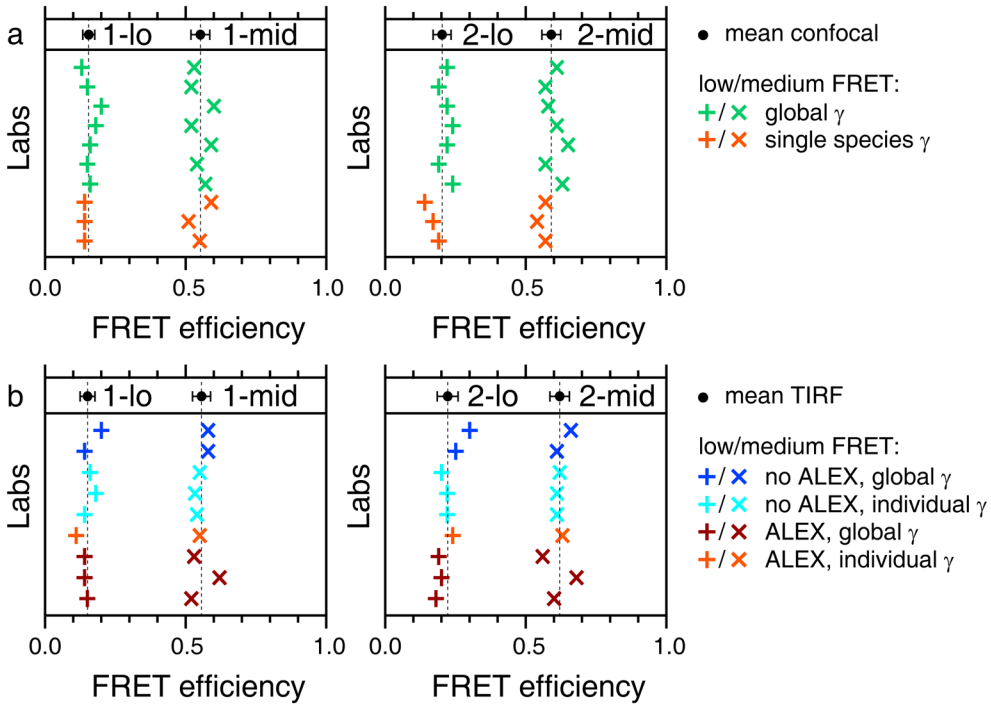

Fig. 3.

Summary of the results of the intensity-based methods. **(a)** Confocal measurements. **(b)** TIRF measurements. Note that some laboratories performed measurement with both methods. In the top panel of each plot, the mean and standard deviations are depicted. Dashed lines indicate the means, their values are summarized in Supplementary Table 4. Example correction factors are given in Supplementary Table 3.

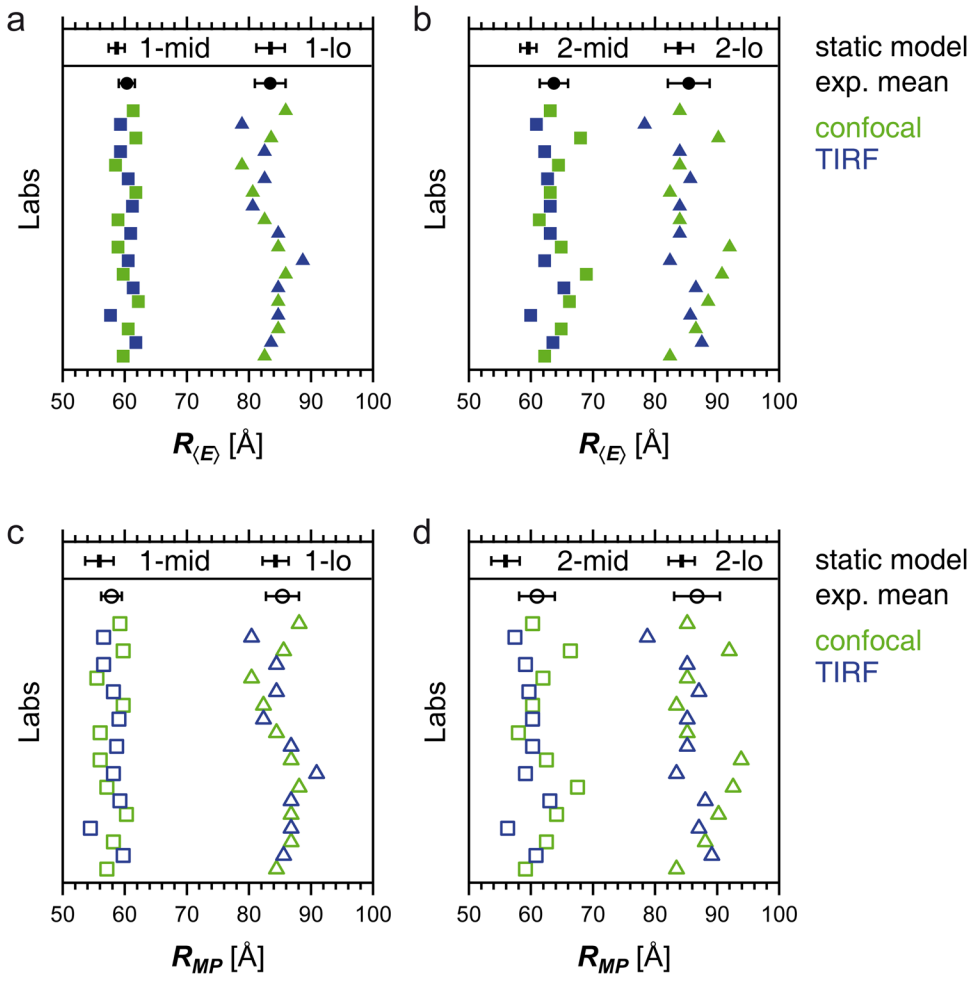

Fig. 4.

Mean inter-dye distances determined from the nineteen ⟨E⟩ values measured in sixteen different labs. **(a)** $R_{\langle E \rangle}$ for sample 1; **(b)** $R_{\langle E \rangle}$ for sample 2; **(c)** R_{MP} for sample 1; **(d)** R_{MP} for sample 2. The black dots (exp. mean) indicate the means and the error bars the statistical error (standard deviation) assuming R_0=62.6 Å and R_0=68.0Å for sample 1 and 2, respectively). The black bars indicate the static model values and their error (determined by variation of model parameters), see main text for details and Supplementary Table 4 for values. Note that the depicted errors only include the statistical variations of the FRET efficiencies, but do not include the error in the Förster radii, thus these errors represent the precision of the measurement, but not the accuracy.

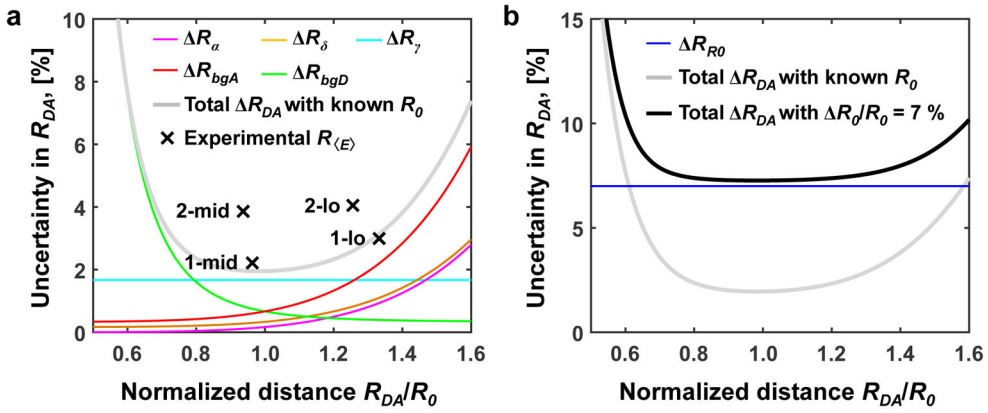

Fig. 5.

Error propagation of experimental uncertainties. **(a)** R_{DA} uncertainty contributions from the experimental correction factors: ΔR_γ (gamma factor), ΔR_{bgD} and ΔR_{bgA} (background), ΔR_α (leakage), ΔR_δ (direct excitation), total uncertainty with known R_0; crosses indicate uncertainty of experimental values of $R_{\langle E\rangle}$ across the labs. See Supplementary Note 6 for details on the error propagation. **(b)** Uncertainty in R_{DA} (black line) based on the efficiency-related uncertainty (bold gray line) and the uncertainty for determining R_0 (blue line). See main text for details. Here we use the following uncertainties, which were determined for the confocal based measurements on sample 1: $\Delta R_0/R_0$=7%, $\Delta\gamma/\gamma$=10%, $\Delta I^{(BG)}/I$=2%, $\Delta\alpha/\alpha$=10% and $\Delta\delta/\delta$=10%. For absolute values see Supplementary Table 3.